

WorldView-2 High Spatial Resolution Improves Desert Invasive Plant Detection

Temuulen Sankey, Brett Dickson, Steve Sesnie, Ophelia Wang, Aaron Olsson, and Luke Zachmann

Abstract

Sahara mustard (Brassica tournefortii) is an invasive species common to the Mojave and Sonoran Deserts in the southwestern US. Our objective was to assess WorldView-2 (wv2) satellite imagery potential to detect Sahara mustard presence, cover, and biomass. We compared wv2 images (2.4 m and 30 m resolution) to Landsat ETM+ image both classified using a mixture tuned matched filtering (MTMF). A total of 1,885 field plots (30 × 30 m) were established across a 8,715 km² study area in spring of 2012, an exceptionally dry year. Average target canopy cover (7.5 percent) and biomass (0.82 g/m²) were extremely low. The wv2 MTMF classification had a much greater overall accuracy of 88 percent, while the resampled wv2 and the Landsat ETM+ MTMF classification overall accuracies were 67 percent and 59 percent, respectively. Producer's and user's accuracies in target detection were 86 percent and 94 percent, respectively, although the exceptionally low canopy cover and biomass were not well correlated with image-based estimates.

Introduction

Non-native plant invasions threaten to alter the structure and function of ecosystems globally (D'Antonio and Vitousek, 1992). Highly invasive plant species can dramatically alter hydrologic and nutrient cycles, fire regimes, and other ecological processes. Invasive plants cost the western US economy as much as 34 billion dollars per year (Barnett *et al.*, 2007). An efficient method to detect and determine the distribution and abundance of non-native invasive plants over large areas is critically needed, particularly for species undergoing rapid expansion in fragile arid ecosystems.

Remote sensing provides a promising tool for targeted monitoring or eradication by land management agencies (Lass *et al.*, 2005; Bradley and Mustard, 2006; Noujdina and Ustin, 2008). Invasive species studies have successfully used hyperspectral data such as AVIRIS imagery with 20 m resolution and 224 bands and HyMap imagery with 3.5 m resolution and 126 bands (O'Neill *et al.*, 2000; Root *et al.*, 2002; Dudek *et al.* 2004; Parker Williams and Hunt, 2002, 2004; Glenn *et al.*, 2005; Noujdina and Ustin, 2008). However, hyperspectral imagery can be expensive to acquire and tends to cover

relatively small spatial extents. Using freely available, moderate resolution imagery such as Landsat can reduce costs and provide data at a temporal resolution suitable for monitoring changes in plant distributions, especially with the recent launch of the Landsat-8 satellite. However, moderate to coarse resolution data typically provide low rates of invasive plant detection because of the mixed cover types within each pixel, especially at early stages of invasion when invasive plant populations are small and sparsely distributed (Lass *et al.*, 2005; Mitchell and Glenn, 2009).

Federal agencies in the US now have access to commercial satellite data such as high resolution WorldView-2 (wv2) imagery using the US Geological Survey Commercial Remote Sensing Space Policy (CRSSP, 2003). Methods to effectively utilize imagery for early detection of invasive species are needed to add value to these data sources as other multispectral and high resolution commercial satellite data become more readily available (Kruse and Perry, 2013). The availability of high resolution data, combined with efficient classification methods for invasive species, can potentially improve early detection rates thereby enhancing invasive species management and mitigation efforts.

The wv2 satellite remote sensing system is a relatively new, high spatial resolution (2.4 m pixels) sensor that is the first of its kind to produce 8-band multispectral imagery (Figure 1) (Kruse and Perry, 2013). wv2 might provide a unique opportunity to detect small populations of desert plants due to its high spatial and spectral resolution and bands in the red (630 to 690 nm), red edge (705 to 745 nm), and near-infrared (770 to 895 nm and 860 to 1040 nm) spectral regions (Figure 1). The fine spatial resolution of wv2 imagery has been demonstrated to improve classification accuracy in forested environments, where overall accuracies reached 98 percent (Ozdemir and Karneli, 2011; Garrity *et al.*, 2012). Latif *et al.* (2012) and Immitzer *et al.* (2012) further document that the high spectral resolution of wv2 imagery result in successful tree species differentiation (overall accuracy of 82 percent), although producer's accuracies at the species-level ranged widely between 33 percent and 92 percent (Immitzer *et al.*, 2012). wv2 data have also been shown to enhance classification accuracy for tree species differentiation in a savanna ecosystem (Cho *et al.*, 2012), cover types in urban areas (Zhang and Kerekes, 2012; Longbotham *et al.*, 2012; Pu and Landry, 2012), and coral reef detection in marine environments (Botha *et al.*, 2013). The utility of wv2 imagery for mapping invasive plants has not been fully explored in hot desert environments where invasive species can exhibit large interannual variability in distribution and abundance.

Temuulen Sankey is with the School of Earth Sciences and Environmental Sustainability, Northern Arizona University, 1298 S. Knoles Drive, Flagstaff AZ 86011. (Temuulen.Sankey@nau.edu).

Brett Dickson, Ophelia Wang, Aaron Olsson, and Luke Zachmann are with the Lab of Landscape Ecology and Conservation Biology, Landscape Conservation Initiative, Northern Arizona University, Box 5694, Flagstaff, AZ 86011, and Conservation Science Partners, Inc., 11050 Pioneer Trail, Suite 202, Truckee, CA 96161.

Steve Sesnie is with the US Fish and Wildlife Service, Albuquerque, NM 87102.

Photogrammetric Engineering & Remote Sensing
Vol. 80, No. 9, September 2014, pp. 885–893.
0099-1112/14/8009–885

© 2014 American Society for Photogrammetry
and Remote Sensing
doi: 10.14358/PERS.80.9.885

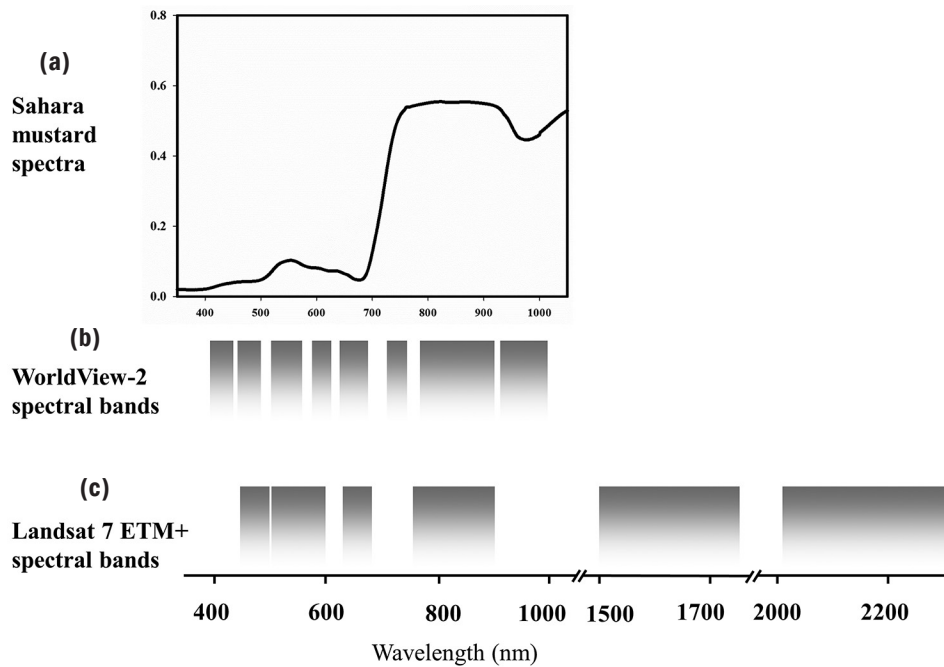


Figure 1. Field-measured mean reflectance spectra of the target species: (a) Sahara mustard, (b) the spectral bands of the WorldView-2, and (c) Landsat ETM+ used in this study.

Our objectives were to: (a) examine the utility of WV2 data for mapping small populations of Sahara mustard in the Sonoran desert of the southwestern US, and (b) compare WV2 classification performance with the more readily available Landsat Enhanced Thematic Mapper Plus (ETM+) imagery. Specifically, we sought to determine if the higher spatial and spectral resolution imagery can improve detection of small populations of invasive plants in desert environments (Figure 1).

Sahara mustard (*Brassica tournefortii*) is a desert winter annual forb that has commonly spread across much of the Mojave and Sonoran deserts of the southwestern US and northern Mexico. Sahara mustard has been identified as one of six invasive species with the greatest potential ecological damage in the Sonoran desert (Sánchez-Flores, 2007). In the context of global and regional climate change, the species is expected to further expand its range. Sahara mustard germinates early in the winter and often reaches maturity before native annuals, which allows it to ultimately replace the native species and dominate a site sometimes with up to 100 percent canopy cover (Sánchez-Flores, 2007; Marushia *et al.*, 2010). Dense stands of Sahara mustard pose a potential fire hazard in desert ecosystems by increasing fine fuels, particularly in locations where native plants are not fire-tolerant or are slow to recover (Engle and Abella, 2012; Balch *et al.*, 2013), and where Sahara mustard can successfully establish following fire from the soil seed bank (Sánchez-Flores, 2007).

Methods

Study Area

Our study was conducted in the lower Sonoran Desert of southwestern Arizona and encompassed an area of approximately 8,715 km² (Figure 2). Study area vegetation is dominated by native plant species typical of the lower Colorado River subdivision (Brown, 1994), including creosote bush (*Larrea tridentata*), palo verde (*Cercidium microphyllum*), jumping cholla (*Opuntia bigelovii*), and brittlebush (*Encelia farinosa*), along with annual grasses and forbs, such as desert sand verbena (*Abronia villosa*),

and evening primrose (*Oenothera caespitosa*). In addition to Sahara mustard, other non-native invasive species of concern in the study area include red brome (*Bromus rubens*), Mediterranean grass (*Schismus arabicus* and *Schismus barbatus*), and arugula (*Eruca vesicaria ssp. sativa*). Annual grasses and forbs in the Sonoran desert typically germinate following winter rains and grow through the months of December to April. Their production is heavily dependent on winter precipitation and can vary dramatically between years and locations (Reynolds *et al.*, 2004). Average annual precipitation across the study area is 93 to 175 mm (PRISM; <http://www.prism.oregonstate.edu>). Average temperatures range between 8° to 40.5°C. Elevation ranges from 25 m to over 1,477 m. The topography is characterized by desert valleys, plains, and bajadas, which are often intersected by xeroriparian (desert wash) features.

Field Measurements

Field data on the presence or absence, cover, and biomass of Sahara mustard was collected at multiple sampling locations between February and April 2012 (Figure 2). Prior to field sampling, the study area was stratified based on a species distribution model for Sahara mustard and a prediction of habitat suitability (Wang *et al.*, *in revision*). Field sampling locations were randomly selected within areas of the 70th percentile of habitat suitability, but confined to areas of low slopes and proximity to improved and unimproved roads. The rationale for selecting areas based on slope (≤ 10 degrees) and proximity to roads (250 m to 2 km) was to reduce the amount of effort required to access field locations and increase sample size in habitats preferred by Sahara mustard. Next, a spatially balanced approach was implemented to identify 2,500 potential sampling locations with a weighted representation of suitable habitats based on predicted habitat suitability across available sampling areas. The approach used specific raster cell values (i.e., weights of habitat suitability) to determine the inclusion probability of a location to be sampled (Stevens and Olsen, 2004; Theobald *et al.*, 2007). Candidate sampling locations were constrained to clusters of four to five locations within 450 to 650 m of one another.

At each sampling location, five 30 × 30 m plots (referred to as “sub-plots” in Wang *et al.*, (in revision)) were generated, each matched to a 30 m Landsat pixel (Figure 3a). Using a global positioning system, we navigated to the southwest corner of each plot (Figure 3a). The entire plot was first searched systematically to determine the presence or absence of the target plant species, Sahara mustard. Next, five 20 m line transects were established within each 30 × 30 m field plot

(Figure 3b). Along each line transect, a point intercept method was used to record the presence or absence of the target species and three other herbaceous cover types: perennial grass, annual grass, and forb (Figure 3b). The point intercept method was used at 1 m intervals resulting in a total of 100 points per plot, which were then directly converted into percent cover estimates of the target species and the three herbaceous cover types at the 30 m plot scale.

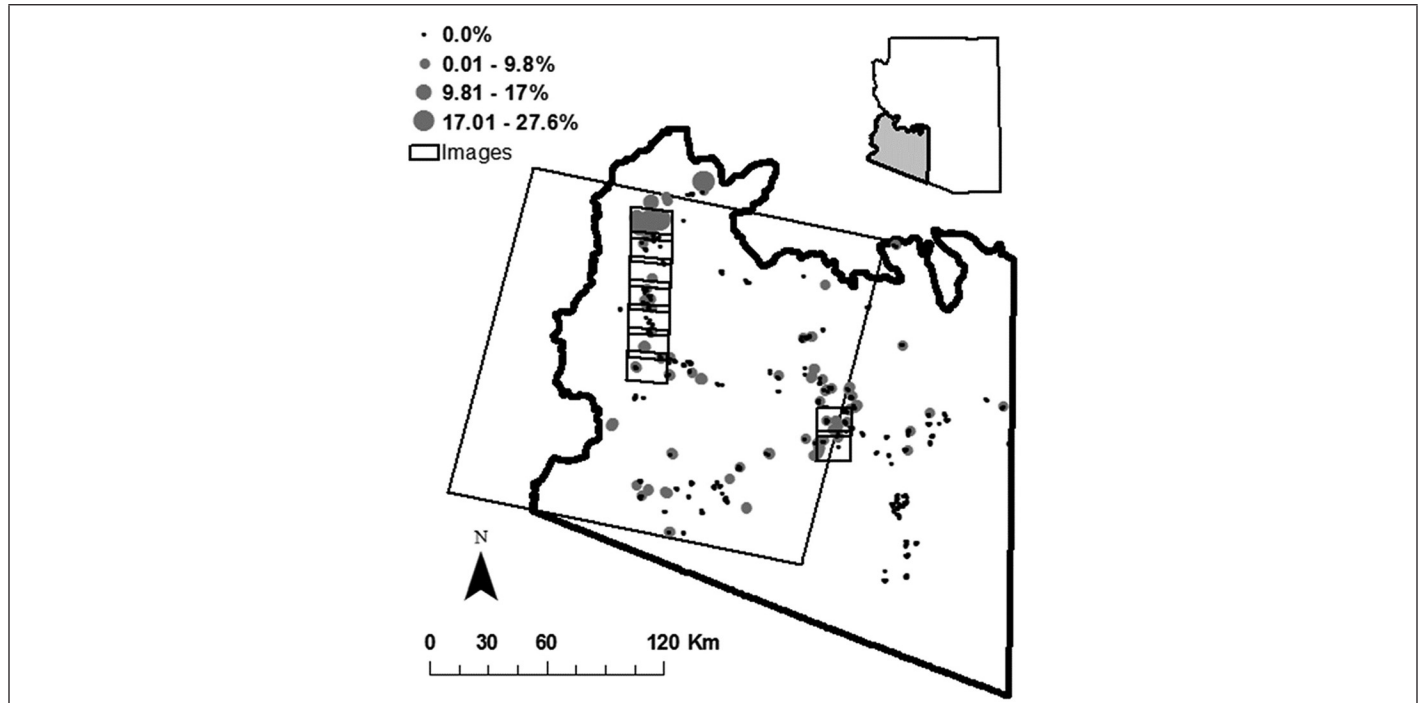


Figure 2. Study area in southwestern Arizona, (inset). The black lines indicate the footprints of the satellite images used in this study: ten scenes of WorldView-2 data overlapping with one Landsat-5 ETM+ image. The circular dots of all sizes demonstrate the spatial distribution of Sahara mustard presence and canopy cover (percent) measured in the field. The size of the dots are proportional to the Sahara mustard canopy cover (percent) measured in the field.

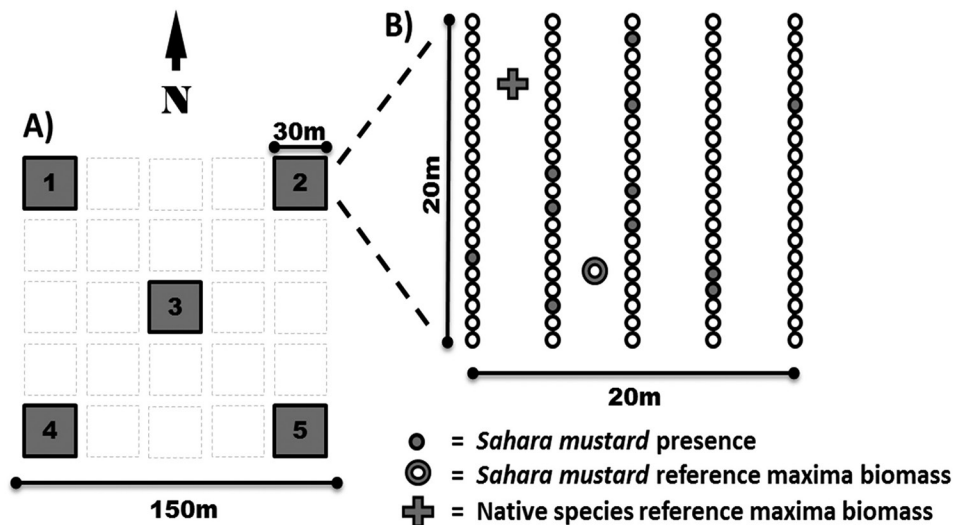


Figure 3. Field sampling design used to detect and measure Sahara mustard canopy cover and biomass: (a) At each sampling location, a cluster of five 30 × 30 m plots were established, each registered to a Landsat image pixel (30 × 30 m); (b) Within each 30 × 30 m field plot, five 20 m line transects were established to record, at 1 m intervals, the presence/absence of the target species (presence highlighted with filled circles) and three other herbaceous cover types: perennial grass, annual grass, and forb (not highlighted). Total herbaceous biomass was approximately estimated within each plot using a modified comparative yield model and a location of reference maxima biomass of the target species (open circle) and native herbaceous species (cross).

Total herbaceous biomass was estimated within each plot using a modified comparative yield method (Haydock and Shaw, 1975). For this estimate, a location of maximum biomass of the target species and native herbaceous species (all native species combined) was found within each plot and labeled as a reference maxima for each (Figure 3b). The biomass of the target species and native herbaceous species were then clipped within a 0.25 m² hoop (BLM, 1996; Despain and Smith, 1997) at the two respective locations. Samples were oven dried and weighed to obtain dry weights of maximum herbaceous biomass for native and non-native plants. In the remainder of each plot, target species and native species biomass were visually ranked as a fraction of the reference maxima biomass in increments of 25 percent at 5 m intervals along the five 20 m transects. The mean of all biomass ranks for each cover type ($n = 20$ points) was then multiplied by the percent cover of each cover type to estimate total herbaceous biomass at the 30 m plot scale.

Image Preprocessing

Imagery from both WV2 and ETM+ satellite sensors were collected during the peak winter growing season period for native and non-native annual plants in the Sonoran Desert. A total of ten WV2 scenes were selected from the study area (Figure 2). The scenes were acquired between 04 to 10 February 04 2012 and delivered in calibrated radiance in 2.4 m resolution with ~5 m geometric accuracy. Multispectral bands were used in this study: coastal (0.477 μm), blue (0.477 μm), green (0.546 μm), yellow (0.607 μm), red (0.658 μm), red edge (0.723 μm), near-infrared 1 (0.831 μm), and near-infrared 2 (0.908 μm) (Figure 1). The swath width of each WV2 scene is 16.4 km. One ETM+ scene (Path 38 and Row 37) from 23 February 2012 encompassing all of the WV2 scenes was used with all bands except band 6 (Figures 1 and 2). Both the WV2 and ETM+ data were corrected for atmospheric effects using the FLAASH module in ENVI image processing software v. 4.8 (ITT Industries Inc., 2008, Boulder, Colorado) and projected in UTM Zone 11N and NAD 1983 projection and datum. The WV2 images were orthorectified using a 10 m digital elevation model (www.ned.usgs.gov). All images were co-registered to orthorectified 2007 NAIP digital imagery (all RMSE were <1 pixel).

NDVI

WV2 data has two near-infrared bands: band 7 (0.831 μm) and band 8 (0.908 μm). This allowed calculations of two separate versions of Normalized Difference Vegetation Index (NDVI) (hereafter referred to NDVI-B7 and NDVI-B8, respectively). NDVI-B7 and NDVI-B8 were calculated using the following equations (Equations 1 and 2) for both WV2 and the resampled WV2. ETM+ NDVI was also calculated using the bands 3 and 4:

$$NDVI = \frac{B5 - B7}{B5 + B7} \quad (1)$$

$$NDVI = \frac{B5 - B8}{B5 + B8} \quad (2)$$

MTMF Classification

Previous studies have recommended sub-pixel classification techniques such as the Mixture-Tuned Matched Filtering (MTMF), when using coarser resolution data such as Landsat TM and ETM+ (Root *et al.*, 2004; Mladinich *et al.*, 2006; Hunt and Parker Williams, 2006). MTMF is a spectral mixture analysis technique which estimates the relative proportion or abundance of a target cover type within each pixel. Spectral mixture analysis techniques are especially useful in arid and semi-arid environments, where a mixture of bare ground and vegetation is common within pixels (Noujiddina and Ustin,

2008; Sankey *et al.*, 2010). Linear spectral mixture analysis produces a mixture which represents a linear combination of the endmembers or cover types weighted by the areal coverage of each endmember in a pixel (Rencz, 1999). Compared to linear spectral unmixing models, MTMF is thought to be better suited for mixed pixels with cover types having similar spectral signatures, because the MTMF suppresses background noise and provides a measure of false positive detection of target cover (Boardman, 1998) that are common in remote sensing of arid and semi-arid vegetation (Okin *et al.*, 2001).

All images from our study area were forward transformed using the Minimum Noise Fraction (MNF) rotation and classified using the MTMF technique in ENVI software to estimate sub-pixel Sahara mustard abundance and ultimately map its presence/absence. The MTMF classification was performed with: (a) WV2 imagery in their original pixel size (hereafter referred to as WV2), (b) WV2 data resampled to 30 m pixel size (hereafter referred to as resampled WV2), and (c) ETM+ image.

An advantage of the MTMF technique is that it requires only endmember training spectra for target species as inputs, but not for background or non-target spectra. Endmember spectra for Sahara mustard was derived from field measurements of 10 healthy green Sahara mustard plant canopy reflectance (350 to 2500 nm) using an ASD, Inc. FieldSpec 3Max spectrometer. A series of five measurements (25 replicates per measurement) were made per plant using a bare fiberoptic cable with a 25° field of view at 45 cm above the plants with dense, closed canopies. Reflectance was calibrated between samples using a non-calibrated diffuse white reference panel (ASD, Inc., Boulder, Colorado). Spectrometer measurements were acquired under clear sky conditions within one hour of solar noon on 24 February 2012. The mean value for all Sahara mustard reflectance spectra was used as a single composite endmember (Figure 1).

The MTMF classification produces two images that can be used together to classify a target cover: (a) matched filtering (MF) scores that estimate the target cover abundance within each pixel, and (b) infeasibility values which represent the likelihood of false positives in the MF scores. In the first image, an MF score near 0 indicates background noise, while a score of 1 corresponds to approximately 100 percent cover of the target spectrum within a pixel. MF scores have been used as direct estimates of sub-pixel target cover abundance and correlated with field-based estimates of target canopy cover where R^2 ranged between 0.32 to 0.69 (Parker Williams and Hunt, 2002; Mundt *et al.*, 2007, Mitchell and Glenn, 2009, Sankey and Glenn, 2011). MF scores, however, tend to underestimate abundance and present a complex mathematical problem (Mitchell and Glenn, 2009) because of its unconstrained estimations within pixels resulting in negative target cover values as well as values greater than 100 percent, which are difficult to correlate to field-based cover estimates that range between 1 and 100 percent. Furthermore, there is no automated method to combine the MF scores with the infeasibility values to reduce false positives in the MF scores. A user defined approach was, therefore, used to produce a final map of the target cover (Mundt *et al.*, 2007).

To determine the best approach to combining the MF scores and infeasibility values, the relationship between the two bands in all images were examined using a regression approach (Sankey *et al.*, 2010). The best fit regression model was then chosen for each image type based on its statistical significance ($\alpha = 0.05$ for all variables), the value of the coefficient of determination (R^2), and model simplicity (i.e., fewer variables were preferred over more complex models with small increases in R^2). The following three quadratic polynomial regression models were chosen to combine the MF scores and the infeasibility values in the WV2, resampled WV2, and ETM+ images, respectively:

$$Y = 2.34 + 22.59*MF + 103.72 *MF^2 \quad (3)$$

$$Y = 2.39 + 28.53*MF + 507.84* MF^2 \quad (4)$$

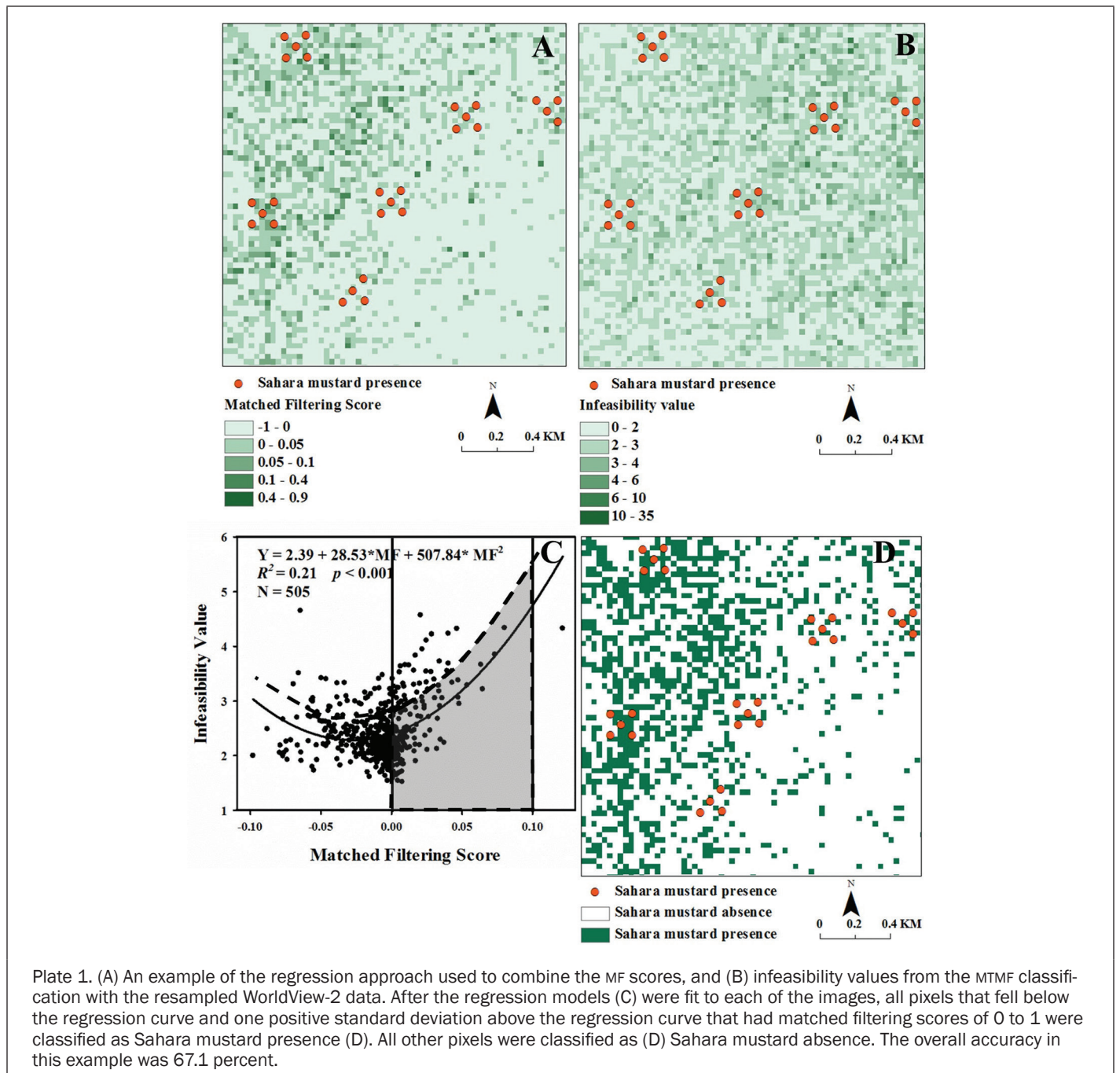
$$Y = 0.64 - 0.97*MF + 0.05* MF^2 \quad (5)$$

where the infeasibility values were the response variable and the MF scores, and quadratic terms were the predictor variables. After the regression models were fit to each image, all pixels that fell below the regression curve and one positive standard deviation above the regression curve and one positive standard deviation above the regression curve that had matched filtering scores of 0 to 1 were classified as Sahara mustard presence (Plate 1). This approach allows the exclusion of negative and >1 MF scores, which do not correlate to the field-based estimates of canopy cover and indicate target cover absence. The regression curve provides an objective

and quantitative approach to determining a threshold in the infeasibility values. The positive standard deviation above the regression curve increases true positive detection by raising the upper limit of the infeasibility values while still limiting unacceptably large infeasibility values and keeping the MF scores within the 0 to 1 range (Sankey *et al.*, 2010). The standard deviation below the regression curve was not used because no minimum threshold was necessary for the low infeasibility values. All other pixels were classified as Sahara mustard absence. As a result, three separate binary maps of Sahara mustard presence/absence were produced: one at 2.4m resolution and two at 30 m resolution.

Accuracy Assessment

First, the binary classifications of Sahara mustard presence/absence were assessed for accuracy (Story and Congalton, 1986) using the field data. The binary map at 2.4 m resolution



was compared to the point data along the line transects (Figure 3b). To represent Sahara mustard presence and absence, 700 points (equally divided between presence and absence) were randomly selected from a total of 27,100 points and from the entire area encompassing the images, which ensured that the selected points were spatially independent minimizing spatial autocorrelation. Furthermore, the field-mapped points were buffered with a 30 m radius to re-enforce a minimum distance between the selected points, because: (a) the point intercept method was used at 1 m intervals along each transect, and therefore, absence and presence points can be potentially found within a single 2.4 m pixel, (b) the GPS horizontal errors ranged up to 6.7 m, and (c) the wv2 data geometric accuracy was 5 m with RMSE <1 pixel. The buffering also insured that absence points with no target species present within a distance of two pixels were selected as absence pixels. The two binary maps at 30 m resolution were compared to an independent set of similarly selected random points of Sahara mustard presence ($n = 370$) and absence ($n = 524$) within the 30 m plots (Figure 3a).

Second, the MF scores were correlated with the field-based Sahara mustard percent cover estimates using a simple linear regression. Only the resampled wv2 and ETM+ MF scores were analyzed, since Sahara mustard percent cover estimates were made at the 30 m plot scale only and no finer scale estimates were available. Sahara mustard percent cover estimates were also divided into three bins with 10 percent incremental increase (i.e., 1 to 10 percent, 10 to 20 percent and >20 percent) to determine if a potential detection threshold existed.

Last, Sahara mustard biomass and the native herbaceous biomass were correlated with the NDVI estimates. The reference maxima biomass measured at the point locations were correlated with the wv2 NDVI estimates, while the Sahara mustard biomass and total herbaceous biomass estimates at the 30 m plot scale were correlated with NDVI estimates from the resampled wv2 and ETM+ (Figure 3b).

Results

Field Measurements

A total of 1,885 plots were established across the study area. Sahara mustard was detected in a total of 748 plots (40 percent). Within these 30 × 30 m plots, Sahara mustard canopy cover averaged 7.5 percent (Table 1). Average reference maxima biomass of Sahara mustard was 2.19 g/m² and the estimated average Sahara mustard biomass at plot scale was 0.82 g/m² (Table 1). The remaining plots had native vegetation species, sometimes mixed with other non-native invasive species. On average, native herbaceous cover was 11 percent. Average reference maxima for native herbaceous biomass was 1.64 g/m² and the average native herbaceous biomass was 1.17 g/m² across all plots.

MTMF Classification of Sahara Mustard Presence and Absence

The wv2 MTMF classification using field collected spectra achieved an overall accuracy of 88 percent. Producer's accuracies were 86 percent and 91 percent for presence and absence, respectively, while user's accuracies were 94 percent and 79 percent (Table 2). The resampled wv2 MTMF classification overall accuracy was 67 percent. Producer's accuracies were 47 percent and 84 percent for presence and absence, respectively (Table 2). User's accuracies were 70 percent and 66 percent for presence and absence, respectively (Table 2). The ETM+ MTMF classification had an overall accuracy of 59 percent. Producer's accuracies were 0 percent and 100 percent for Sahara mustard presence and absence, respectively, while user's accuracies were 0 percent and 59 percent (Table 2).

TABLE 1. STATISTICAL DESCRIPTIONS OF THE SAHARA MUSTARD DISTRIBUTION OBSERVED IN 748 FIELD PLOTS (30 × 30 M) FROM A TOTAL OF 1,885 FIELD PLOTS ACROSS THE STUDY AREA

Variables measured	Mean	Minimum	Maximum
Canopy cover	7.5%	0%	41%
Reference maxima biomass	2.19 g/m ²	0.004 g/m ²	19.29 g/m ²
Estimated biomass	0.82 g/m ²	0 g/m ²	11.66 g/m ²

TABLE 2. ACCURACY ASSESSMENT OF SAHARA MUSTARD PRESENCE AND ABSENCE CLASSIFICATION USING WORLDVIEW-2, RESAMPLED WORLDVIEW-2, AND LANDSAT ETM+ IMAGES

Image sources	Producer's accuracy		User's accuracy		Overall accuracy
	Presence	Absence	Presence	Absence	
WorldView-2	86%	91%	94%	79%	88%
Resampled WorldView-2	47%	84%	70%	66%	67%
Landsat ETM+	0%	100%	0%	59%	59%

MF Scores and Sahara Mustard Abundance Estimate

The wv2 scenes overlapped with 136 plots (30 × 30 m) with Sahara mustard canopy cover estimates. Of these plots, 102 had target cover abundance of 1 to 10 percent. Target detection rate in these plots were 58 percent. A total of 29 plots had target cover abundance of 10 to 20 percent, while only five plots had >20 percent target cover abundance. These two bins were, therefore, combined into a single bin of >10 percent abundance. Target detection rate in the combined bin of >10 percent abundance was similar at 57 percent. When wv2 MF scores were correlated with Sahara mustard percent cover estimates, the coefficient of determination (R^2) was extremely low at 0.004 with p -values of 0.473 and 0.011 for MF scores and infeasibility values, respectively. Many of the MF scores were negative values. When only the pixels with positive MF scores were correlated with Sahara mustard canopy cover estimates, the regression coefficient of determination was also only 0.06, but MF scores were a significant predictor variable (p -values of 0.002 and 0.264 for MF scores and infeasibility values, respectively). The R^2 increased substantially to 0.21, when NDVI-B7 was added to the regression model as a predictor variable ($p < 0.001$). The R^2 further increased to 0.36, when a second NDVI-B8 ($p < 0.001$) was added to the model.

The ETM+ MF scores produced a low coefficient of determination (R^2) of only 0.02, when correlated with Sahara mustard percent cover estimates. The MF scores were a significant predictor variable ($p = 0.04$), although infeasibility values were not ($p = 0.51$) ($n = 1,465$). When only the plots with Sahara mustard canopy cover estimates >1 percent were correlated with the MF score ($n = 266$), the R^2 was 0.08 ($p < 0.001$ and 0.74 for MF scores and infeasibility values, respectively). The R^2 value did not increase, when NDVI was added to the regression model as a predictor variable ($p = 0.20$).

NDVI and Sahara Mustard Biomass

wv2 NDVI-B7 and NDVI-B8 each produced R^2 values of only 0.03 ($p < 0.001$), when correlated with field-measured Sahara mustard biomass at point locations. Resampled wv2 NDVI-B7 and NDVI-8 each had an R^2 of 0.16 when regressed with Sahara mustard biomass estimated at the 30 m plot scale ($p = 0.015$ and 0.010, respectively). A similar result was obtained when the same NDVIs were regressed with total native herbaceous biomass. ETM+ NDVI produced an R^2 of 0.002 ($p = 0.46$) when regressed with Sahara mustard biomass.

Discussion

WV2 Imagery and Invasive Plant Detection

Previous studies of desert vegetation have largely used moderate-coarse resolution data and concluded that much of the variability in desert vegetation cover remains unexplained (Casady *et al.*, 2013). Successful remote sensing applications in desert environments have only provided a “proxy” of photosynthetic green vegetation dynamics and coarse-resolution pulses of vegetation green-up (Wallace and Thomas, 2008). Our study provides the first quantitative evaluation of desert invasive plant detection for the newly available, high-resolution WV2 data. Considering the challenges in a desert environment, the performance of WV2 data was sufficient for detecting small populations of Sahara mustard in a dry year with relatively low plant productivity. Sahara mustard presence/absence mapping with WV2 data produced an overall accuracy of 89 percent. This is similar to the accuracies presented in other studies that have tested WV2 data in other environments. WV2 thematic classification overall accuracy was 82 percent in a forested environment (Immitzer *et al.*, 2012), 77 percent in a savanna environment (Cho *et al.*, 2012), between 57 to 100 percent in an urban classification (Zhang and Kerekes, 2012), and 63 percent in an urban tree species classification (Pu and Landry, 2012). While most of the previous WV2 classification studies focused on broad land-cover types, some of the studies tested WV2 utility in individual species classification. Producer’s accuracies for individual tree species mapped with these studies ranged from 65 to 82 percent (Cho *et al.*, 2012), 33 to 94 percent (Immitzer *et al.*, 2012), to 16 to 75 percent (Pu and Landry, 2012), while producer’s accuracy for Sahara mustard in this study was 86 percent.

WV2 data appears to provide a large improvement in accuracies for detecting invasive plant populations in desert environments over moderate resolution satellite data. The WV2 application in this study produced almost 30 percent greater accuracies over ETM+ classification. We attribute the increase in accuracy largely to the high spatial resolution of WV2 data. This is evidenced by the performance and lower classification accuracy of the resampled WV2 data. The WV2 data resampled to 30 m pixels produced 20 percent lower accuracy compared to the original WV2 data, although the same bands, field spectra, and classification approach were used. The resampled WV2 binary classification of Sahara mustard presence and absence and sub-pixel abundance estimates had similar performance to the ETM+ data. This likely indicates that the higher spatial resolution of WV2 data provides a key advantage in hot desert environments (Wallace and Thomas, 2008; Casady *et al.*, 2013) where invasive plant populations can become sparse during extremely dry periods, but rapidly expand in favorable conditions. While target detection methods such as MTMF benefit from the high spatial resolution, sub-pixel vegetation abundance estimates remain to be a major challenge in these ecosystems even with a greater number of spectral bands. Future studies should be aimed at estimating sub-pixel plant abundance by refining field sampling techniques more suitable to the WV2 original pixel size.

Desert vegetation is often distributed in small diffuse patches during dry years and their spectral signature is largely overwhelmed by the prominent reflectance from bare ground and geologic substrates (Shupe and Marsh, 2004). At the 30 m plot scale in this study, average percent cover estimates of Sahara mustard and other herbaceous classes were extremely low at 7.5 percent and 11 percent, respectively. Taken together, the total herbaceous cover is still less than the proposed detectable limit of 30 percent and 40 percent vegetation cover in desert environments with hyperspectral and multispectral Landsat TM data, respectively (Okin *et al.*, 2001; Smith *et al.*, 1990). The ETM+ MTMF classification performed poorly at this

level of vegetation abundance, although MTMF is a sub-pixel mapping method specifically developed to enhance target detection (Rencz, 1999). The ETM+ MTMF accuracy from this study is similar to a previous Landsat TM-based invasive detection application in the Sonoran desert, where accuracies ranged between 35 to 65 percent (Olsson *et al.*, 2011). Although ETM+ MTMF overall accuracy was 59 percent in this study, MF scores were extremely low and MTMF did not detect any Sahara mustard presence given the low canopy cover in our study area.

WV2 Imagery and Herbaceous Plant Biomass

This study provides the first quantitative evaluation of high resolution WV2 data for estimating invasive and native winter annual biomass in an arid desert environment. These results can provide key information for land management strategies, including the appropriate response to fire, which has become more common in this region of the Southwest in recent decades (Esque *et al.*, 2013). Winter annual plants, such as the non-native Sahara mustard, are a primary source of fine fuels in hot desert environments (Brooks and Pyke, 2001). Unlike the extremely dry year sampled in this study, winter periods with above-average precipitation can be followed by large increases in annual native and non-native vegetation biomass and fine fuels, which significantly increases fire risk in a desert environment (Esque *et al.*, 2013; Gray *et al.*, (in review)). Timely remote sensing assessment of desert fine fuels can, therefore, provide an important tool for land managers to monitor or mitigate damaging fire events in native vegetation communities of the southwestern US.

Despite its high spatial and spectral resolution, WV2 NDVI appears to perform poorly in annual vegetation biomass estimates in arid desert environments during extremely dry periods such as the spring 2012 sampled in this study, although WV2 performance in annual vegetation biomass estimates might be greater in average and above-average winter precipitation years. The observed poor performance might be due to the georegistration errors in the image and the point locations of biomass data resulting in mismatched individual pixels with point locations. WV2 imagery offers two near-infrared bands allowing two separate calculations of NDVI. The two NDVI estimates, however, appear to both correlate poorly with field-measured annual vegetation biomass and offer no unique advantage under the extremely low productivity conditions characteristic of this study area during the dry year sampled. WV2 NDVI estimates appear to produce similar results to ETM+ NDVI and previous coarse-resolution satellite image applications in desert environments. Casady *et al.* (2013) found that the relationship between winter annual biomass and MODIS NDVI in the Sonoran and Mojave deserts produced R^2 ranging between 0.19 to 0.25 when excluding one productive site from their model. Wallace and Thomas (2008) demonstrated R^2 of 0.47 when correlating annual plant canopy cover and MODIS EVI data in the Mojave desert.

To accommodate relatively high temporal and spatial variability in winter annual biomass in southwestern desert ecosystems, previous studies propose time-series applications in which pixels are compared to extremely dry years (Wallace and Thomas, 2008) or locations (Casady *et al.*, 2013) to calculate relative winter annual biomass. Similarly, multitemporal WV2 data might produce better results than a single date of imagery (Marshall *et al.* 2012). In future studies, we seek to explore multi-temporal WV2 data using the proposed methods to better capture temporal variability in winter annual vegetation biomass. We believe contrasting image dates of high and low annual productivity periods could likely produce better results than the moderate and coarse resolution time-series data, given the high spatial resolution and the promising results from the binary classification in this study.

Conclusions

This study demonstrates that WV2 imagery can perform well in detecting small populations of invasive plants in a desert ecosystem of the southwestern US. In particular, WV2 image sub-pixel classification using the MTF technique performs well in mapping winter annual invasive species, namely Sahara mustard. We attribute the successful performance to the high spatial resolution of WV2 data. In comparison, resampled WV2 and ETM+ image classification using the same technique produced poor classification accuracies. These datasets also performed poorly in predicting Sahara mustard canopy cover and biomass at the 30 m plot scale. Similarly, the high-resolution WV2 had a low correlation with field-measured biomass at point locations. Although quantitative estimates of vegetation canopy cover and biomass during extremely dry years remain a challenge in arid ecosystems even with high resolution data, WV2 data analysis may perform better in years of average and high precipitation.

Acknowledgements

This research was supported by the Strategic Environmental Research and Development Program (SERDP) project ID RC-1722 and Joint Fire Science Program project ID 10-1-04-07. Thanks to the Bureau of Land Management, US Fish and Wildlife Service National Wildlife Refuge System, Organ Pipe Cactus National Monument, Tohono o'dham Nation, US Army Yuma Proving Ground and the Barry M. Goldwater Air Force Range, who helped facilitate data collection for this study.

References

- Asner, G.P., M.O. Jones, R.E. Martin, D.E. Knapp, and R. F. Hughes, 2008. Remote sensing of native and invasive species in Hawaiian forests, *Remote Sensing of Environment*, 112:1912–1926.
- Balch, J.K., B.A. Bradley, C.M. D'Antonio, and J. Gomez-Dans, 2013. Introduced annual grass increases regional fire activity across the arid western USA (1980-2009), *Global Change Biology*, 19:173–183.
- Barnett, D.T., T.J. Stohlgren, C.S. Jarnevich, G.W. Chong, J.A. Ericson, T.R. Davern, and S.E. Simonson, 2007. The art and science of weed mapping, *Environmental Monitoring Assessment*, 132:235–252.
- Botha, E., V.E. Brando, J.M. Anstee, A.G. Dekker, and S. Sagar, 2013. Increased spectral resolution enhances coral detection under varying water conditions, *Remote Sensing of Environment*, 131:247–261.
- Boardman, J.W., 1998. Leveraging the high dimensionality of AVIRIS data for improved sub-pixel target unmixing and rejection of false positives: Mixture tuned matched filtering, *Proceedings of AVIRIS 1998*, JPL, Pasadena, California, 6 p.
- Bradley, B.A., 2013. Distribution models of invasive plants over-estimate potential impact, *Biological Invasions*, 15:1417–1429.
- Bradley, B.A., and J.F. Mustard, 2005. Identifying land cover variability distinct from land cover change: Cheatgrass in the Great Basin, *Remote Sensing of Environment*, 94:204–213.
- Bradley, B.A., and J.F. Mustard, 2006. Characterizing the landscape dynamics of an invasive plant and risk of invasion using remote sensing, *Ecological Applications*, 16:1132–1147.
- Brooks M.L., and D.A. Pyke, 2001. Invasive plants and fire in the deserts of North America, *Proceedings of the Invasive Plant Workshop: The Role of Fire in The Control and Spread of Invasive Species* (K. Galley and T. Wilson, editors), Tallahassee, Florida, (Tall Timbers Research Station: Tallahassee, Florida), pp 1–14.
- Brown, D.E., 1994. *Biotic Communities: Southwestern United States and Northwestern Mexico*, University of Utah Press, Salt Lake City, Utah.
- Bureau of Land Management, 1996. *Sampling Vegetation Attributes. Interagency Technical Reference*, BLM/RS/ST-96/002p1730, Denver, Colorado: BLM National Applied Resources Sciences Center, pp. 112–121.
- Casady, G.M., W.J.D. Leeuwen, and B.C. Reed, 2013. Estimating winter annual biomass in the Sonoran and Mojave deserts with satellite- and ground-based observations, *Remote Sensing*, 5:909–926.
- Cho, M.A., R. Mathieu, G.P. Asner, L. Naidoo, J. Aardt, A. Ramoelo, P. Debba, K. Wessels, R. Main, I. P.J. Smit, and B. Erasmus, 2012. Mapping tree species composition in South African savannas using an integrated spectral and LiDAR system, *Remote Sensing of Environment*, 125:214–226.
- CRSSP, 2003. *U.S. Commercial Remote Sensing Space Policy: Civil Agency Implementation Plan*, URL: <http://crssp.usgs.gov/pdfs/CRSSPplan121203.pdf> (last date accessed: 02 July 2014).
- D'Antonio, C.M., and P.M. Vitousek, 1992. Biological invasions by exotic grasses, the grass fire cycle, and global change, *Annual Review of Ecology and Systematics*, 23:63–87.
- Despain, D.W., and E.L. Smith, 1997. The comparative yield method for estimating range production, *Some Methods for Monitoring Rangelands* (G.B. Ruyle, editor), Tucson, Arizona, University of Arizona Cooperative Extension Report 9043, pp. 49–61.
- Dudek, K.B., R.R. Root, R.F. Kokaly, and G.L. Anderson, 2004. Increased spatial and temporal consistency of leafy spurge maps from multitemporal AVIRIS imagery: A hybrid linear spectral mixture analysis/mixture-tuned matched filtering approach, *Proceedings of the 13th JPL Airborne Earth Science Workshop*, 21 March-02 April 2004. Pasadena, California, NASA Jet Propulsion Laboratory.
- Engle, E.C., and S.R. Abella, 2011. Vegetation recovery in a desert landscape after wildfires: Influences of community type, time since fire and contingency effects, *Journal of Applied Ecology*, 48:1401–1410.
- Esque, T.C., R.H. Webb, C.S.A. Wallace, C. van Riper III, and L. Smythe, 2013. Desert fires fueled by native annual forbs: Effects of fire on communities of plants and birds in the lower Sonoran Desert of Arizona, *The Southwestern Naturalist*, 58:223–233.
- Garrity, S.R., C.D. Allen, S.P. Brumby, C. Gangodagamage, N.G. McDowell, and D.M. Cai, 2013. Quantifying tree mortality in a mixed species woodland using multitemporal high spatial resolution satellite imagery, *Remote Sensing of Environment*, 129:54–65.
- Glenn, N.F., J.T. Mundt, K.T. Weber, T.S. Prather, L.W. Lass, and J. Pettingill, 2005. Hyperspectral data processing for repeat detection of small infestations of leafy spurge, *Remote Sensing of Environment*, 95:3549–3564.
- Gray, M.E., B.G. Dickson, and L.J. Zachmann, In Review. Modeling and mapping dynamic variability in large fire risk in the lower Sonoran Desert of the southwestern Arizona, *International Journal of Wildland Fire*.
- Haydock, K., and N. Shaw, 1975. The comparative yield method for estimating dry matter yield of pasture, *Animal Production Science*, 15:663–670.
- Hunt, E.R., and A.E. Parker Williams. 2006. Detection of flowering leafy spurge with satellite multispectral imagery, *Rangeland Ecology and Management*, 59:494–499.
- Immitzer, M., C. Atzberger, and T. Koukal, 2012. Tree species classification with Random Forest using very high spatial resolution 8-band WorldView-2 satellite data, *Remote Sensing*, 4:2661–2693.
- Kruse, F.A., and S.L. Perry, 2013. Mineral mapping using simulated WorldView-3 short-wave-infrared imagery, *Remote Sensing*, 5:2688–2703.
- Laliberte, A.S., M.A. Goforth, C.M. Steele, and A. Rango, 2011. Multi-spectral remote sensing from unmanned aircraft: image processing workflows and applications for rangeland environments, *Remote Sensing*, 3:2529–2551.
- Lass, L.W., T.S. Prather, N.F. Glenn, K.T. Weber, J.T. Mundt, and J. Pettingill, 2005. A review of remote sensing of invasive weeds and example of the early detection of spotted knapweed (*Centaurea maculosa*) and babysbreath (*Gypsophila paniculata*) with a hyperspectral sensor, *Weed Science*, 53:242–251.
- Latiff, Z.A., I. Zamri, and H. Omar, 2012. Determination of tree species using WorldView-2 data. *Proceedings of IEEE 8th International Colloquium on Signal Processing and its Applications*, pp. 383–387.

- Longbotham, N., C. Chaapel, L. Blieler, C. Padwick, W. Emery, and F. Pacifici, 2012. Very high resolution multi-angle urban classification analysis, *IEEE Transactions on Geoscience and Remote Sensing*, 50:1155–1170.
- Marsett, R.C., J. Qi, P. Heilman, S. Biedenbender, M. Watson, S. Amer, M. Weltz, D. Goodrich, and R. Marsett, 2006. Remote sensing for grassland management in the arid southwest, *Rangeland Ecology and Management*, 59:530–540.
- Marshall, V., M. Lewis, and B. Ostendorf, 2012. Do additional bands (coastal, NIR-2, red-edge, and yellow) in WorldView-2 multispectral imagery improve discrimination of an invasive tussock, buffel grass (*Cenchrus ciliaris*)?, *International Archives of the Photogrammetry, Remote Sensing and Spatial Information Sciences*, XXII ISPRS Congress, 25 August - 01 September, Melbourne, Australia.
- Marushia, R.G., M.W. Cadotte, and J.S. Holt, 2010. Phenology as a basis for management of exotic annual plants in desert invasions, *Journal of Applied Ecology*, 47:1290–1299.
- Mladinich, C.S., M.R. Bustos, S. Stitt, R. Root, K. Brown, G.L. Anderson, and S. Hager, 2006. The use of Landsat 7 Enhanced Thematic Mapper Plus for mapping leafy spurge, *Rangeland Ecology and Management*, 59:500–506.
- Mitchell, J.J., and N.F. Glenn, 2009. Subpixel abundance estimates in mixture-tuned matched filtering classifications of leafy spurge (*Euphorbia esula* L.), *International Journal of Remote Sensing*, 30:6099–6119.
- Mundt, J.T., D.R. Streutker, and N.F. Glenn, 2007. Partial unmixing of hyperspectral imagery: Theory and methods, *Proceedings of the ASPRS Annual Conference, 2007*, Tampa, Florida, American Society of Photogrammetry and Remote Sensing, unpaginated CD-ROM.
- Noujdina, N.V., and S.L. Ustin, 2008. Mapping downy brome (*Bromis tectorum*) using multivariate AVIRIS data, *Weed Science*, 56:173–179.
- Okin, G.S., D.A. Roberts, B. Murray, and W. Okin, 2001. Practical limits on hyperspectral vegetation discrimination in arid and semiarid environments, *Remote Sensing of Environment*, 77:212–225.
- Okin, G.S., K. Clarke, and M.M. Lewis, 2013. Comparison of methods for estimation of absolute vegetation and soil fractional cover using MODIS normalized BRDF-adjusted reflectance data, *Remote Sensing of Environment*, 130:266–279.
- Olsson, A.D., W.J.D. Leeuwan, and S.E. Marsh, 2011. Feasibility of invasive grass detection in a desertscrub community using hyperspectral field measurements and Landsat TM imagery, *Remote Sensing*, 3:2283–2304.
- O'Neill, M., S.L. Ustin, S. Hager, and R. Root, 2000. Mapping the distribution of leafy spurge at Theodore Roosevelt National Park using AVIRIS, *Proceedings of the Ninth JPL Airborne Earth Science Workshop* (R. D. Green, editor), Pasadena, California, NASA Jet Propulsion Laboratory.
- Ozdemir, I., and A. Karnieli, 2011. Predicting forest structural parameters using the image texture derived from WorldView-2 multispectral imagery in a dryland forest, Israel, *International Journal of Applied Earth Observation and Geoinformation*, 13:701–710.
- Parker Williams, A.E., and E.R. Hunt, 2002. Estimation of leafy spurge cover from hyperspectral imagery using mixture tuned matched filtering, *Remote Sensing of Environment*, 82:446–456.
- Parker Williams, A.E., and E.R. Hunt, 2004. Accuracy assessment for detection of leafy spurge with hyperspectral imagery, *Journal of Range Management*, 57:106–112.
- Pu, R., and S. Landry, 2012. A comparative analysis of high spatial resolution IKONOS and WorldView-2 imagery for mapping urban tree species, *Remote Sensing of Environment*, 124:516–533.
- Rencz, A.N., 1999. *Remote Sensing for the Earth Sciences*, Wiley and Sons, New York, pp. 251–307.
- Reynolds, J.F., P.R. Kemp, K. Ogle, and R.J. Fernandez, 2004. Modifying the 'pulse-reserve' paradigm for deserts of North America: Precipitation pulses, soil water, and plant responses, *Oecologia*, 141:194–210.
- Root, R.R., G.L. Anderson, S.N. Hager, K.E. Brown, K.B. Dudek, and R.F. Kokaly, 2004. Application of advanced remote sensing and modeling techniques for the detection and management of leafy spurge: challenges and opportunities, *Proceedings of the Society for Range Management 57th Annual Meeting*, 24–30 January, Salt Lake City, Utah and Denver, Colorado, Society for Range Management.
- Sánchez-Flores, E., 2007. GARP modeling of natural and human factors affecting the potential distribution of *Schismus arabicus* and *Brassica tournifortii* in 'El Pinacate y Gran Desierto de Altar' Biosphere Reserve, *Ecological Modeling*, 204:457–474.
- Sankey, T.T., and N.F. Glenn, 2011. Landsat-5 TM and lidar fusion for sub-pixel juniper tree cover estimates, *Photogrammetric Engineering & Remote Sensing*, 77(12):1241–1248.
- Sankey, T.T., N. Glenn, S. Ehinger, A. Boehm, and S. Hardegree, 2010. Characterizing western juniper expansion via a fusion of Landsat-5 Thematic Mapper and lidar data, *Rangeland Ecology and Management*, 63:514–523.
- Shupe, S.M., and S.E. Marsh, 2004. Cover- and density-based vegetation classifications of the Sonoran Desert using Landsat TM and ERS-1 SAR imagery, *Remote Sensing of Environment*, 93:131–149.
- Smith, M.O., S.L. Ustin, J.B. Adams, and A.R. Gillespie, 1990. Vegetation in deserts: I - A regional measure of abundance from multispectral images, *Remote Sensing of Environment*, 31:1–26.
- Smith, M.O., S.L. Ustin, J.B. Adams, and A.R. Gillespie, 1990. Vegetation in deserts: II - Environmental influences on regional abundance, *Remote Sensing of Environment*, 31:27–52.
- Stevens Jr., D.L., and A.R. Olsen, 2004. Spatially balanced sampling of natural resources, *Journal of the American Statistical Association*, 99:262–278.
- Story, M., and R.G. Congalton, 1986. Accuracy assessment: A user's perspective, *Photogrammetric Engineering & Remote Sensing*, 52(3):397–399.
- Theobald, D.M., D.L. Stevens, D. White, N.S. Urganhart, A.R. Olsen, and J.B. Norman, 2007. Using GIS to generate spatially balanced random survey designs for natural resource applications, *Environmental Management*, 40:134–146.
- Underwood, E., S. Ustin, and D. DiPietro, 2003. Mapping nonnative plants using hyperspectral imagery, *Remote Sensing of Environment*, 86:150–161.
- Wallace, C., and K.A. Thomas, 2008. An annual plant growth proxy in the Mojave Desert using MODIS-EVI data, *Sensors*, 8:7792–7808.
- Wang, O., L.J. Zackmann, S.E. Sesnie, A.D. Olsson, and B.G. Dickson. A targeted sampling design information by habitat suitability models for detecting focal plant species over extensive areas, *PLOS ONE*, (In revision).
- Zhang, J., and J. Kerekes, 2012. Unsupervised urban land-cover classification using WorldView-2 data and self-organizing maps, *Proceedings of IEEE 8th International Colloquium on Signal Processing and its Applications*, pp.150–153.

(Received 09 December 2013; accepted 28 February 2014; final version 13 May 2014)